

# The effect of inhomogeneities on the distance to the last scattering surface and the accuracy of the CMB analysis

Krzysztof Bolejko

Astrophysics Department, University of Oxford, 1 Keble Road, Oxford OX1 3RH, UK

**Abstract.** The standard analysis of the CMB data assumes that the distance to the last scattering surface can be calculated using the distance-redshift relation as in the Friedmann model. However, in the inhomogeneous universe, even if  $\langle \delta\rho \rangle = 0$ , the distance relation is not the same as in the unperturbed universe. This can be of serious consequences as a change of distance affects the mapping of CMB temperature fluctuations into the angular power spectrum  $C_l$ . In addition, if the change of distance is relatively uniform no new temperature fluctuations are generated. It is therefore a different effect than the lensing or ISW effects which introduce additional CMB anisotropies. This paper shows that the accuracy of the CMB analysis can be impaired by the accuracy of calculation of the distance within the cosmological models. Since this effect has not been fully explored before, to test how the inhomogeneities affect the distance-redshift relation, several methods are examined: the Dyer–Roeder relation, lensing approximation, and non-linear Swiss-Cheese model. In all cases, the distance to the last scattering surface is different than when homogeneity is assumed. The difference can be as low as 1% and as high as 80%. Excluding extreme cases, the distance changes by about 20 – 30%. Since the distance to the last scattering surface is set by the position of the CMB peaks, in order to have a good fit, the distance needs to be adjusted. After correcting the distance, the cosmological parameters change. Therefore, a not properly estimated distance to the last scattering surface can be a major source of systematics. This paper shows that if inhomogeneities are taken into account when calculating the distance then models with positive spatial curvature and with  $\Omega_\Lambda \sim 0.8 - 0.9$  are preferred. The  $\Lambda$ CDM model (i.e. a flat Friedmann solution with the cosmological constant), in most cases, is at odds with the current data.

## 1. Introduction

It has been said that we entered the era of precision cosmology. This is mainly due to observations of the cosmic microwave background radiation (CMB). As the CMB power spectrum is very sensitive to cosmological parameters it provides very tight constraints. Currently the errors are at the level of a few percent [1]. The CMB power spectrum is shaped by several processes that can be divided into two groups. The first group involves processes that occurred before and during the generation of the CMB. This part is well understood as the Universe at that times was very close to homogeneous and contribution from the spatial curvature and dark energy was negligible. The constraints

on cosmological parameters coming just from this group of processes were recently presented and discussed in [2]. The second group of processes takes into account what happens with photons between the last scattering surface and the observer. This includes the distance to the last scattering surface, the ISW effect, the impact of reionization on the CMB, the Sunyaev-Zel'dovich and the lensing effects.

The analysis of this second group of effects is a subject to systematics, as the geometry of the late time Universe does not have to be close to homogeneous and isotropic Robertson-Walker geometry (these processes are most often studied within the framework of linear perturbations around the homogeneous Friedmann models). On small scales (say  $\ell > 60$ , i.e.  $\theta < 3^\circ$ ), except for the distance, these processes should not significantly modify the overall shape of the CMB power spectrum. The distance to the last scattering surface affects the mapping of CMB temperature fluctuations into the angular power spectrum  $C_\ell$ . This effect can be modelled by introducing the shift parameter  $\mathcal{R}$ , which is proportional to the distance to the last scattering surface [3, 4]. Therefore, there is a number of papers where the constraints from the CMB are just limited to the constraints on the shift parameter. This is usually done when testing different models of dark energy [5, 6], alternative cosmological models [7, 8], or Gpc-scale inhomogeneous models [9, 10, 11, 12, 13, 14, 15, 16, 17, 18]. As discussed in [19, 20] this type of analysis can be improved but taking into account both the scale of the sound horizon at the last scattering and  $\mathcal{R}$ .

This paper studies the effect of the distance but does not consider any alternative cosmologies. Here we just focus on the effect of small-scale inhomogeneities on the distance to the last scattering. The presence of inhomogeneities is known to affect the distance-redshift relation [21, 22]. Some studies claim that the effect is large [23, 24, 25, 46], others that it is small [27, 28, 29, 30, 31]. Even if the change of the distance just at the level of a few percent [32, 33, 34, 35] this analysis is still important as a change of the distance by a few percent leads to a similar change of the inferred values of cosmological parameters.

One may think that the effect of inhomogeneities is taken into account in the standard analysis of the CMB via the ISW or lensing effects. However, in both cases (in the standard approach) this is done by using the matter power spectrum. Thus, this analysis is insensitive to the change of the mean, i.e. the uniform change of the distance to the last scattering surface. For example the lensing analysis deals with the change of the distance but is only sensitive to the change of the variance, not the mean (cf. [36, 37]). If the change of distance is relatively uniform (i.e. with a negligible variance) then no additional temperature anisotropies are generated. Since the change of distance affects the mapping of the physical position of the peaks to the peaks in the angular power spectrum  $C_\ell$  this effect needs to be considered also at the level of the mean.

Therefore, if inhomogeneities are not taken into account when calculating the distance, then they may become a major source of systematics. With the increasing precision of CMB experiments, in particular Planck, a proper understanding of systematics is important. Without taking into account all systematics the precision

cosmology will not be an accurate cosmology. Therefore, this paper aims to study how the presence of inhomogeneities affects the distance-redshift relation, in particular the distance to the last scattering surface. Several models are considered and it is shown that the change of distance due to inhomogeneities is not negligible.

The structure of this paper is as follows: Sec. 2 discusses different methods for the distance calculation, Sec. 3 applies these methods to calculate the distance to the last scattering surface, Sec. 4 explores the implication of differences in the distance, and Sec. 5 concludes the results.

## 2. Distance and distance corrections

As shown by Sachs [21], the equation for the angular diameter distance  $D_A$  is

$$\frac{d^2 D_A}{ds^2} = -(|\sigma|^2 + \frac{1}{2} R_{\alpha\beta} k^\alpha k^\beta) D_A, \quad (1)$$

where  $s$  is a parameter along the geodesic,  $k^\alpha$  is a null vector that is tangent to the geodesic,  $\sigma$  is the shear of the light bundle,  $R_{\alpha\beta}$  is the Ricci tensor and  $R_{\alpha\beta} k^\alpha k^\beta = \kappa T_{\alpha\beta} k^\alpha k^\beta$ . In the comoving and synchronous coordinates, for pressure-less matter,  $R_{\alpha\beta} k^\alpha k^\beta = \kappa \rho k^0 k^0$ . As seen, the distance depends on density fluctuations, and secondly, even if the perturbations vanish after averaging (i.e.  $\langle \rho \rangle = \langle \rho_0 + \delta \rho \rangle = \rho_0$ , where  $\rho_0$  is the background density) they do modify the distance relation and the final result deviates from the homogeneous solution. Equation (1) is the differential equation so it is sensitive to any change of initial conditions. Therefore, it is sensitive to  $\delta \rho D_A$  as this term acts as a potential (for a detailed discussion see [34]). As the parameter  $s$  is not directly measured (unless the geodesic parametrization is chosen in a particular way), it is convenient to express it in terms of a redshift. The redshift is given by the following relation [38]

$$1 + z = \frac{(u_\alpha k^\alpha)_e}{(u_\alpha k^\alpha)_o}, \quad (2)$$

where  $u^\alpha$  is the 4-velocity, and subscripts  $e$  and  $o$  refer to emission and observation instants respectively. In the comoving and synchronous coordinates  $u^\alpha = \delta_0^\alpha$  and

$$1 + z = \frac{k_e^0}{k_o^0},$$

where  $k^0 = dt/ds$ . Thus, for a given model and using the above relation the parameter  $s$  can be replaced with  $z$ .

### 2.1. Homogeneous universe

When homogeneity is assumed, i.e.  $\sigma = 0 = \delta \rho$ , and  $k^0 = 1/a$  (where  $a(t)$  is the scale factor) then  $dz/ds = -(1+z)^2 H_0 \sqrt{\Omega_m(1+z)^3 + \Omega_k(1+z)^2 + \Omega_\Lambda}$  and (1) reduces to

$$D_A(z) = \frac{1}{H_0(1+z)\sqrt{-\Omega_k}} \sin \left( \int_0^z dz' \frac{\sqrt{-\Omega_k}}{\sqrt{\Omega_m(1+z')^3 + \Omega_k(1+z')^2 + \Omega_\Lambda}} \right), \quad (3)$$

where  $H_0$  is the Hubble constant,  $\Omega_k = -k/(H_0^2 a_0^2)$ ,  $\Omega_m = (8\pi G\rho_0)/(3H_0^2)$ , and  $\Omega_\Lambda = \Lambda/(3H_0^2)$ .

## 2.2. Dyer–Roeder approximation

The Dyer–Roeder approach also assumes homogeneity but takes into account that light propagates through vacuum. Therefore,  $\Omega_m$  which photons ‘feel’ is different than true  $\Omega_m$ . This is modelled by a constant parameter  $\alpha$  (of value between 0 and 1) that multiplies  $\Omega_m$ . In this case (1) reduces to [39, 40, 41]

$$\frac{d^2 D_A}{dz^2} + \left( \frac{1}{H} \frac{dH}{dz} + \frac{2}{1+z} \right) \frac{dD_A}{dz} + \frac{3}{2} \frac{H_0^2}{H^2} \alpha \Omega_m (1+z) D_A = 0, \quad (4)$$

where  $H(z) = H_0 \sqrt{\Omega_m(1+z)^3 + \Omega_k(1+z)^2 + \Omega_\Lambda}$ . In order to include the evolution of density fluctuations along the line of sight, Ref. [35] suggests the following modification of the Dyer–Roeder equation

$$\frac{d^2 D_A}{dz^2} + \left( \frac{1}{H} \frac{dH}{dz} + \frac{2}{1+z} \right) \frac{dD_A}{dz} + \frac{3}{2} \frac{H_0^2}{H^2} \Omega_m (1+z) \left( 1 + \frac{\langle \delta \rangle_{1D}}{(1+z)^{5/4}} \right) D_A = 0, \quad (5)$$

where  $\langle \delta \rangle_{1D}$  is the mean of the present-day density fluctuations along the line of sight.

Initial conditions needed to solve (4) and (5) are:  $D_A(0) = 0$  and  $dD_A/dz = 1/H_0$ .

## 2.3. Linear perturbations and the lensing approximation

Within the linear perturbative scheme the distance is

$$D_A(z) = \bar{D}_A(1 + \Delta_D), \quad (6)$$

where  $\bar{D}_A$  the distance in the homogeneous universe and is given by (3). The most general form for  $\Delta_D$  is presented in [42, 43, 44, 45]. Neglecting the contribution from the observer’s and source’s motion, and taking the leading term,  $\Delta_D$  can be expressed as

$$\Delta_D = - \int_0^{\chi_e} d\chi \frac{\chi_e - \chi}{\chi_e} \chi \nabla^2 \phi(\chi), \quad (7)$$

where  $\chi$  is the comoving coordinate  $d\chi = dz/H(z)$ ,  $\phi$  is the gravitational potential that relates to the density perturbations  $\delta\rho$  via the Poisson equation  $\nabla^2 \phi = \frac{4\pi G}{c^2} a^2 \delta\rho$ . The above expression is equivalent to the convergence in the lensing approximation and is known as the Born approximation. As seen, propagation through voids ( $\delta\rho < 0$ ) increases the distance while propagation through overdense regions ( $\delta\rho > 0$ ) decreases the distance.

In order to solve (7) one needs to know exactly what the density fluctuations along the line of sight are. However, within the weak lensing analysis one does not solve (7) directly. Instead the variance is calculated, thus instead of  $\delta\rho$  one has  $(\delta\rho)^2$  which can be expressed in terms of the matter power spectrum. In this paper we are interested in the



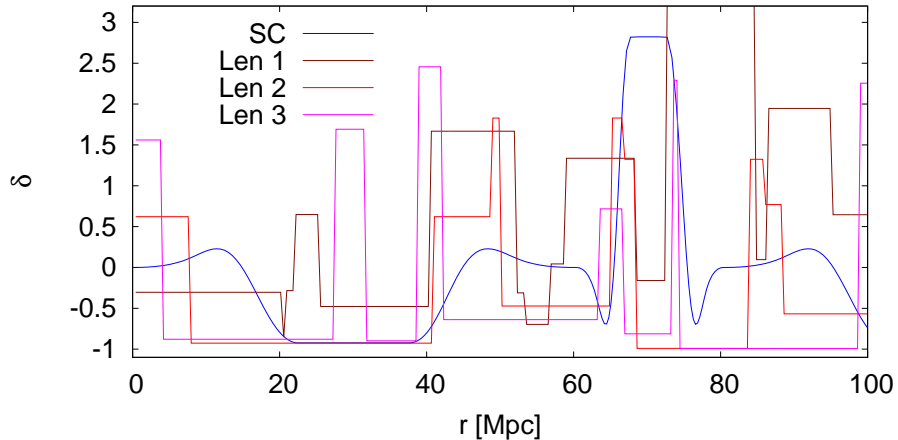


**Figure 1.** Density fluctuations along the line of sight within the lensing approximation and the Swiss Cheese model.

overall (uniform) change of the distance. Thus, we will solve (7) directly, this requires knowledge of density fluctuations along the line of sight. The algorithm is described below, but see also [46, 47] for an alternative approach.

### 3. Distance to the last scattering surface

To test what is the effect of inhomogeneities on the distance to the last scattering surface and the accuracy of the CMB analysis, let us consider 7 different ways of calculating the distance to the last scattering surface

- (i) The  $\Lambda$ CDM model:  
Distance to the last scattering surface is calculated from (3).
- (ii) Dyer–Roeder approximation (model DR):  
Based on the cosmological observations, Yu et al. [48] suggest that  $\alpha = 0.93$ . Therefore, the distance to the last scattering surface is calculated using (4) with  $\alpha = 0.93$ .
- (iii) Modified Dyer–Roeder relation (model mDR):  
The modified version of the Dyer–Roeder equation (5) is solved with  $\langle \delta \rangle_{1D} = -0.3$ .
- (iv) Lensing approximation (model Len 1):  
In order to solve (7), one needs to know  $\nabla^2 \phi$  along the line of sight. Using the Poisson equation the gravitational potential is related to density fluctuations. The density fluctuations along the line of sight are generated from the log-normal PDF – the algorithm is discussed in details in Appendix A.
- (v) Lensing approximation (model Len 2):  
In model Len 1 the mean of density fluctuations along the line of sight is negligible. However, as pointed out in [35] the mean of density fluctuations along the line of sight does not have to vanish, as  $\langle \delta \rangle_{3D} = 0$  (3D – volume average) does not

necessarily imply  $\langle \delta \rangle_{1D} = 0$  (1D – along the line of sight). In model Len 2,  $\langle \delta \rangle_{1D} \neq 0$  although  $\langle \delta \rangle_{3D} = 0$ . The algorithm is discussed in details in Appendix B.

(vi) Lensing approximation (model Len 3):

Model Len 3 uses a more flexible (than Len 1 & 2) method of generating density fluctuations along the line of sight. The algorithm is presented in details in Appendix C.

(vii) Fully non-linear model (model SC):

The above approaches were based either on the assumption of homogeneity (the  $\Lambda$ CDM and Dyer–Roeder relation) or on the linear approximation (models Len 1–3). In fact, the lensing approximation is not even fully linear, as it takes into account just the leading linear term. Also, when generating fluctuations along the line of sight, the matching conditions were not taken into account, i.e. the structures were not properly matched. In addition, the light rays were not properly match as well, i.e. when light ray exits one structure and enters another one, the null geodesics need to be properly matched. Therefore, a fully non-linear model is considered here, where the distance is calculated directly from (1) and all matching conditions are handled properly. The model is based on the Swiss-Cheese model. Each inhomogeneous patch is of spherical symmetry and is described using the Lemaître-Tolman (LT) model [49, 50]. Thus, density within each inhomogeneous patch changes continuously, unlike in the lensing approximation, where within each generated structures, matter density is constant. Also the evolution of matter is calculated using the exact method, not the linear approximation. The properties of the model are chosen so that the mean of density fluctuations along the line of sight is zero, i.e.  $\langle \delta \rangle_{1D} \approx 0$ . Thus, this model allows us to test how large non-linear contributions are, in contrast to  $\langle \delta \rangle_{1D} \neq 0$  contributions. The detailed description of this model is presented in Appendix D.

In this section it will be assumed that the large-scale universe is exactly the  $\Lambda$ CDM, so  $H_0 = 71.4 \text{ km s}^{-1} \text{ Mpc}^{-1}$ ,  $\Omega_m = 0.262$ ,  $\Omega_\Lambda = 0.738$ . A sample of density fluctuations along the line of sight is presented in Figure 1. The results, in the form of  $D_A(z)$ , are presented in Figure 2. The distance to the last scattering surface is presented in the inset, and in the form of the shift parameter  $\mathcal{R}$  in the 2nd column of Table 1. As seen, the distance to the last scattering surface depends on the choice of the method. Even within the most optimistic case, model Len 1, the change is of order of 1%. However, the non-linear contributions (even if  $\langle \delta \rangle_{1D} \approx 0$ ) gives  $\sim 30\%$  change of the distance. When  $\langle \delta \rangle_{1D} \neq 0$ , even within the lensing approximation the change is of order of 20 – 30%.

Another important fact is that the variance within each method is small. Models Len 1–3 allow for random (within the limits of the method) density fluctuations along the line of sight. Based on 100,000 runs (each with a different distribution of density fluctuations along the line of sight) the results are Len 1:  $\Delta_D = -0.0071 \pm 0.0198$ , Len 2:  $\Delta_D = 0.2033 \pm 0.0064$ , Len 3:  $\Delta_D = 0.2729 \pm 0.0071$ . This shows that the change of distance is relatively uniform. Below, when referring to models Len 1-3 it will be

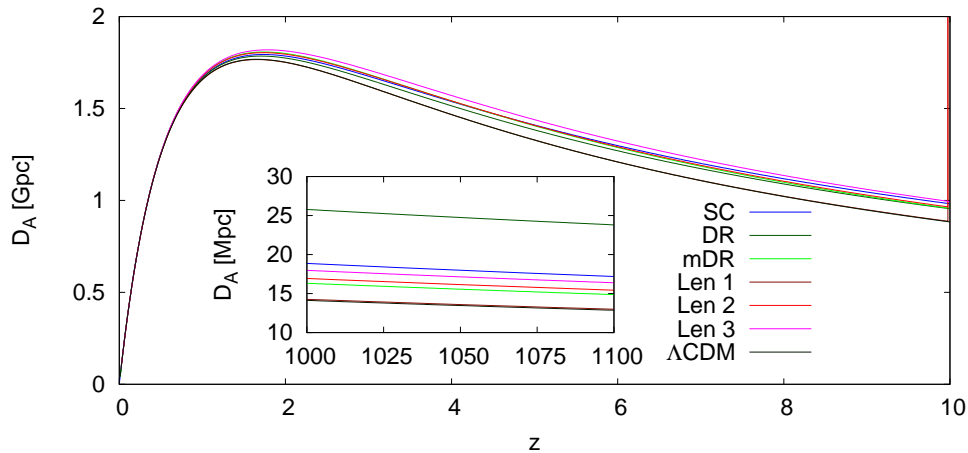


**Figure 2.** The angular diameter distance within 7 considered models. The inset presents  $D_A$  in the vicinity of the last scattering surface.

referred to the mean of  $\Delta_D$  ‡.

In the next section we will study the implications of the change of the distance to the last scattering surface and the CMB constraints when this change is taken into account.

## 4. CMB analysis with the adjusted distance-redshift relation

### 4.1. Fitting the distance and the accuracy of CMB analysis

In this section we assume that the physical densities of baryonic and cold dark matter, and primordial power spectrum are the same as in the standard cosmological model, and only implications of the change of the distance to the last scattering surface are going to be examined.

The change of the distance-redshift relation leads to a different mapping of the CMB temperature fluctuations into the angular power spectrum  $C_\ell$ . Thus, if the distance-redshift relation changes, then the standard analysis of the CMB needs to be adjusted. The way to do this is following: first the CMB power spectrum is calculated using standard codes (for example CAMB [51]) then the output requires following scaling

$$\ell \rightarrow \ell(1 + \Delta_D) \quad \text{and} \quad C_\ell \rightarrow C_\ell(1 + \Delta_D)^{-2}. \quad (8)$$

Thus, the  $\ell$  axis changes while the amplitude  $\ell(\ell + 1)C_\ell$  remains relatively unchanged (for a detailed discussion see [12, 2, 15]). To present how it works let us consider the following example: let us change the value of  $\Lambda$  in such a way so that the distance to the last scattering instant, for studied models, is the same as in the standard cosmological

‡ It should be noted that the distance corrections depends on cosmological parameters of the background model, for example  $\Delta_D$  for model Len 1 changes to  $-0.0064$  and  $-0.0069$  when parameters are as in Table 1 and Table 2 respectively.

model.  $\Omega_\Lambda$  needed to fit the distance, for studied models, is presented in the 3rd column of Table 1. Apart from model Len 1,  $\Omega_\Lambda$  is much larger than when homogeneity is assumed. If the power spectrum was calculated for a homogeneous Friedmann model (i.e. with the distance-redshift relation the same as in the Friedmann model) the result would look like the one presented in Figure 3. However, after applying scaling (8) the angular power spectrum is as in Figure 4. As seen the CMB power spectrum is very similar except for low- $\ell$  where the ISW effect is different. The low- $\ell$  power spectrum is presented in the inset, where the error-bars are enlarged to include the cosmic variance  $\Delta C_\ell/C_\ell = \pm(2/(2\ell + 1))^{1/2}$ .

Another example: let us correct the distance by changing the cosmological parameters but keeping the spatial curvature zero, i.e.  $\Omega_m + \Omega_\Lambda = 1$ . Thus, the change of  $\Omega_m$  automatically implies the change of  $\Omega_\Lambda$ . Also to keep the shape of the CMB power spectrum unchanged,  $\Omega_m h^2 = (\Omega_b + \Omega_c) h^2$  must not change, so the change of  $\Omega_m$  automatically implies the change of  $H_0$ . The change of cosmological parameters needed to fit the distance is presented in Table 2. As seen all models except for model Len 1 can be ruled out because of too high amplitude of  $H_0$ . Even within model Len 1, the change of parameters is large compared to the current precision – for example in model Len 1,  $\Omega_m$  is around 0.28 not 0.262 so the difference is around 7%, which is twice as large as the error estimated by the WMAP team [1]. For completeness the CMB power spectrum for Len 1 and the  $\Lambda$ CDM model are presented in Figure 5.

The above examples show why it is important to have an accurate method for calculating the distance. As the universe is inhomogeneous, the distance-redshift relation is different than the distance-redshift relation in the Friedmann model. As shown, even a small change of the distance can have a large impact on the accuracy of the CMB analysis. As seen from Table 1 a change of the distance by 1% leads to the 0.5% change of the cosmological constant. Although this change is small, in the era of precision cosmology this may be important. Especially that as shown in Table 2 if one puts by hand the assumption of spatial flatness, then systematics are much larger.

#### 4.2. Spatial curvature of the Universe

Let us now focus only on models Len 1, Len 2, and SC. We exclude the Dyer–Roeder relation as this is only a rough approximation (as the shear accumulates along geodesics this approximation is expected to be inaccurate for large distances). Also as model Len 3 is rather of arbitrary matter fluctuations (it was considered only to check how arbitrariness of matter fluctuations changes the results) it is excluded from the further and more detailed analysis.

In this section we will only focus on Len 1, Len 2, and SC models. Len 1 model is a conservative approach – it is based on the linear approach with random density fluctuations along the line of sight. Len 2 model is also based on linear approximation, but the mean of density fluctuations along the line of sight is non-zero (as discussed in [35] if structures in the universe are organized, then density fluctuations are no

**Table 1.** The effect of inhomogeneities on the distance to the last scattering surface – 2nd column ( $\mathcal{R} = D_A(1+z)\sqrt{\Omega_m}H_0/c$ ); the accuracy of estimation of  $\Lambda$  – 3rd and 4th column. In all models  $H_0 = 71.4 \text{ km s}^{-1} \text{ Mpc}^{-1}$ ,  $\Omega_c h^2 = 0.1107$ ,  $\Omega_b h^2 = 0.0227$ .

Model	the shift parameter $\mathcal{R}$ (if the background model is the $\Lambda$ CDM model)	$\Omega_\Lambda$ needed to fit the CMB	$\delta_\Lambda =  \Delta\Omega_\Lambda /\Omega_\Lambda$
$\Lambda$ CDM	1.73	0.738	0.0
Len 1	1.71	0.734	0.005
Len 2	2.08	0.797	0.08
Len 3	2.19	0.802	0.09
SC	2.31	0.919	0.24
DR	3.19	1.071	0.45
mDR	2.04	0.823	0.12

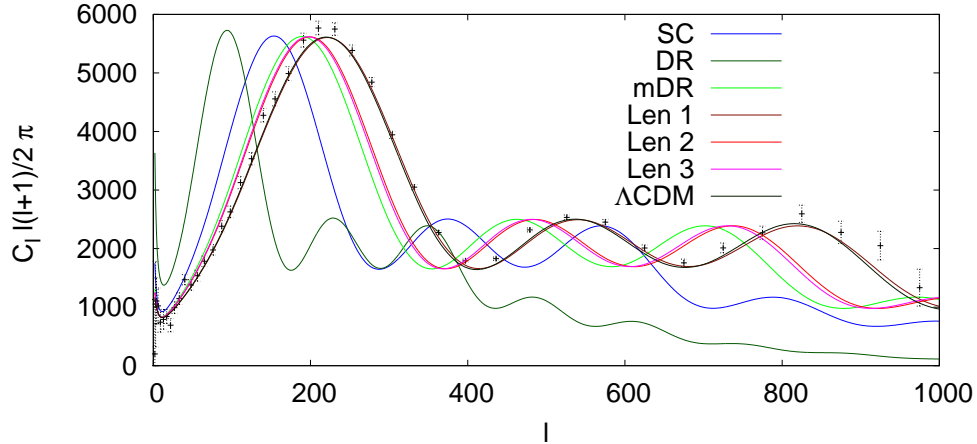


**Figure 3.** The CMB power spectrum calculated with CAMB [51] for homogeneous cosmological models with parameters as in Table 1.

**Table 2.** The effect of inhomogeneities on the accuracy of inferred cosmological parameters. In all models  $\Omega_c h^2 = 0.1107$ ,  $\Omega_b h^2 = 0.0227$ , and  $\Omega_m + \Omega_\Lambda = 1$ .

Model	$\Omega_m$	$\delta_m =  \Delta\Omega_m /\Omega_m$	$\Omega_\Lambda$	$\delta_\Lambda =  \Delta\Omega_\Lambda /\Omega_\Lambda$	$h$	$\delta_h =  \Delta h /h$
$\Lambda$ CDM	0.262	0	0.738	0	0.714	0
Len 1	0.281	0.07	0.719	0.03	0.690	0.03
Len 2	0.050	0.81	0.95	0.29	1.64	1.30
Len 3	0.034	0.87	0.966	0.31	1.982	1.78
SC	0.024	0.91	0.976	0.32	2.344	2.28
DR	0.006	0.98	0.994	0.35	4.568	5.40
mDR	0.095	0.64	0.905	0.23	1.19	0.66

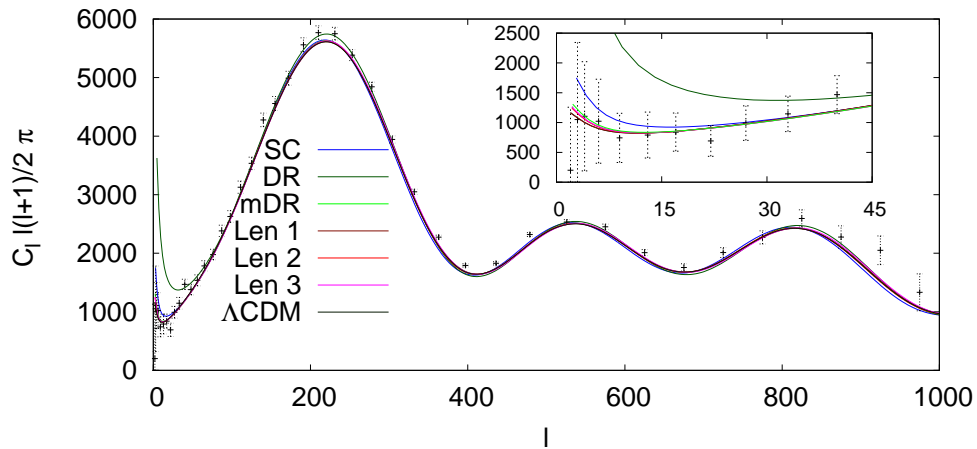


**Figure 4.** The CMB power spectrum calculated with CAMB [51] and corrected for the distance (i.e. with the scaling (8) employed). The inset presents the power spectrum for low- $\ell$  with errors enlarged to include the cosmic variance.

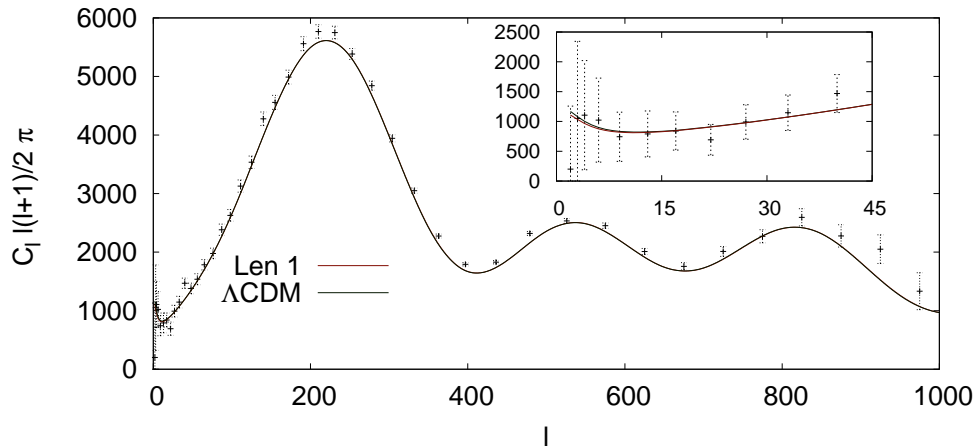


**Figure 5.** The CMB power spectrum calculated with CAMB [51] and corrected for the distance (i.e. with the scaling (8) employed). The inset presents the power spectrum for low- $\ell$  with errors enlarged to include the cosmic variance.

longer purely random, hence even though the 3D average vanish, the average of density fluctuations over the the line of sight is not zero). SC model is a fully non-linear model with vanishing density fluctuations along the line of sight.

The results of the CMB analysis within these 3 models is presented in Fig. 6. Now we allow  $\Omega_m$  and  $\Omega_\Lambda$  to vary freely (however, we keep  $\Omega_b h^2$  and  $\Omega_c h^2$  unchanged, so the change of  $\Omega_m$  implies the change of  $H_0$ ). As seen the constraints obtained within Len 1 model are very similar to the constraints obtained within the standard cosmological model. However, model Len 1 does not include non-linear corrections. If these are taken into account or if only the mean of density fluctuations along the line of sight does not vanish then spatial curvature cannot be zero. As seen the presence of small-scale non-

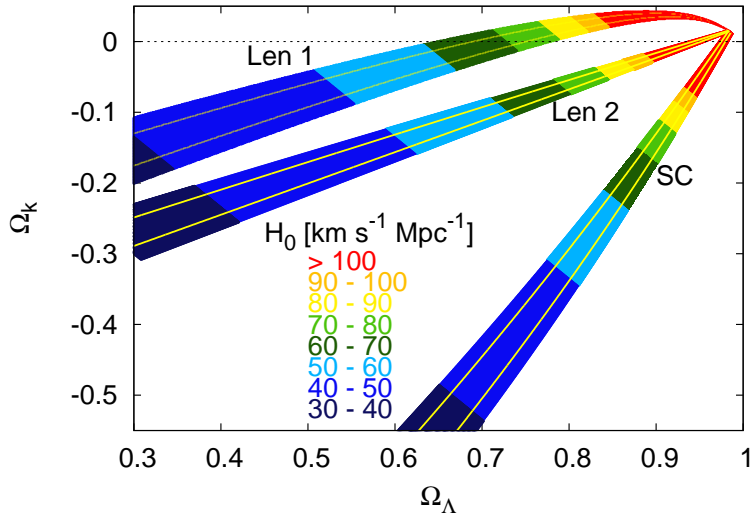


**Figure 6.** The CMB constraints after taking into account the effect of inhomogeneities on the distance to the surface of last scattering, for Len 1, Len 2, and SC models. The color regions are the 95% confidence interval, the yellow lines indicate the 68% confidence interval.

linear structures changes the distance-redshift relation and now the CMB data combined with local value of  $H_0$  no longer favors spatially flat models. This shows that the flat Friedmann solution is not preferred by the data, and when inhomogeneities are included into the distance-redshift relation then  $k > 0$  models with larger amount of dark energy are favored.

Let us discuss for a moment the possibility that in fact  $\Omega_\Lambda \approx 0.8$ . What are the implications? In this case, the age of the universe increases to approximately 14 Gyr. This change is acceptable. An increased amount of dark energy should be detectable by other cosmological observations. The supernova data alone are not very precise, but still homogeneous Friedmann models that fit the data best are the elliptic, not flat, models with  $\Omega_\Lambda \approx 0.9$  [52]. Also, the BAO analysis is in the agreement with larger amount dark energy. However, it should be noted that one of the elements of the BAO analysis is a conversion from the redshift to distance. This conversion is obtained using the Friedmann models. Therefore, if the distance-redshift relation is changed then the result of the BAO analysis can also be different. This should be kept in mind when analyzing the BAO data, especially that as shown in [34] ignoring inhomogeneities also leads to additional systematics.

## 5. Conclusions

This paper investigated how the presence of inhomogeneities (small-scale inhomogeneities observed in the Universe) affects the distance to the surface of last scattering, and how via the change of the distance the inhomogeneities influence the CMB data.

In the standard approach, the distance is calculated within a framework of homogeneous Friedmann models. There are several reasons for using this approach. First of all, there is an argument used by Weinberg [53] who pointed out that although for a single case the distance is modified by the inhomogeneities, but due to photon conservation, when averaged over large enough angular scales the overall effect is zero (however see [54] for an argument why Weinberg’s reasoning should not apply). Second of all, as seen from (7) if the amount of voids is the same as amount of overdensities then  $\Delta_D$  should be zero and the distance should be exactly the same as in the Friedmann model. As density fluctuations should vanish after averaging over sufficiently large scales it seems reasonable to expect that the Friedmann distance-redshift relation correctly describes the reality.

However, there is a difference between vanishing 3D average and vanishing of the average of the density fluctuations over the line of sight. If density fluctuations in the Universe are purely random then vanishing 3D average implies vanishing average over the line of sight. If density fluctuations are not purely random, i.e. if there is some degree of organization, then vanishing 3D average does not necessarily imply vanishing density fluctuations over the line of sight (for a discussion see [35]). As the large-scale matter distribution in the Universe has a form of the cosmic web, there is some kind of organization, and thus the result of (7) does not have to be zero, even if 3D average of density fluctuations vanishes after averaging over sufficiently large scales. This is the case of model Len 2. Also, relation (7) does not apply when structures are non-linear. The calculations within model SC were carried out within the non-linear regime. In addition matter distribution was chosen so that the density fluctuations along the line of sight vanish after averaging (i.e.  $\langle \delta \rangle_{1D} = 0$ ). In this case, again, the distance was not the same as within the Friedmann model.

Even if the change of the distance is small, like in Len 1 model, still the effect is important, as we have already entered the era of precision cosmology – as seen from Table 1 and Table 2 the change of the inferred cosmological parameters, even for Len 1 model, can be of order of a percent or more. If the change of the distance is larger, for example as in models Len 2 and SC, then the inferred parameters are significantly different. In this case spatially flat models are ruled out and the data favors positively curved models with  $\Omega_\Lambda \approx 0.8 - 0.9$ .

As discussed in Sec. (3), within a chosen method, the distance to the last scattering surface is relatively uniform with only small variance. The presented, in this paper, results show that the change of the mean is important, and the proper handling of this effect is essential, otherwise the systematics may be larger than the precision of measurements. The only problem, however, is to have a good method for the calculation of the distance. All models presented in this paper have their limitations, and should rather be treated as toy models, i.e. as examples to show the significance of the problem. The results show that the accuracy of the CMB analysis strongly depends on the accuracy of the calculation of the distance corrections. Peebles described the importance of accuracy and precision in cosmology with the following example *a digital scale may*



read out the weight of an object to many significant figures, in a precise measurement. But if the scale is not well calibrated the measurement may not be very accurate [55]. In our case, the ‘calibration’ requires an inhomogeneous framework that will allow us to estimate the distance with inhomogeneities taken into account. As the non-linear corrections are important this cannot be done within the lensing approximation (7) but requires a fully inhomogeneous framework. Only then we will be able to accurately predict the distance and say: ‘the distance is larger by 29.72%’ or ‘36.14% than when homogeneity is assumed’. With the increasing precision of CMB experiments, in particular Planck, Atacama Cosmology Telescope, and South Pole Telescope this is important. Otherwise, what would be the meaning of a measurement with very high precision ( $\sim 1\%$  statistical errors) if the accuracy is low ( $\sim 30\%$  systematics)?

## Acknowledgments

I would like to thank Richard Bond, Chris Clarkson, Timothy Clifton, Ruth Durrer, Pedro Ferreira, Valerio Marra, Teppo Mattsson, Syksy Räsänen, Marco Regis, David Wiltshire for useful discussions and suggestions. This research of was supported by the Marie Curie Fellowship (PIEF-GA-2009-252950).

## References

- [1] Komatsu E, Smith K M, Dunkley J, Bennett C L, Gold B, et al 2010, arXiv:1001.4538
- [2] Vonlanthen M, Räsänen S, Durrer R 2010 *J. Cosmol. Astropart. Phys.* JCAP08(2010)023
- [3] Bond J R, Efstathiou G, Tegmark M 1997 *Mon. Not. R. Astron. Soc.* **291** L33
- [4] Efstathiou G, Bond J R, 1999 *Mon. Not. R. Astron. Soc.* **304** 75
- [5] Melchiorri A, Mersini L, Ödman C J, Trodden M 2003 *Phys. Rev. D* **68** 043509
- [6] Kurek A, Szydlowski M 2008 *Astrophys. J.* **675** 1
- [7] Lazkoz R, Maartens R, Majerotto E 2006 *Phys. Rev. D* **74** 083510
- [8] Rydbeck S, Fairbairn M, Goobar A 2007 *J. Cosmol. Astropart. Phys.* JCAP05(2007)003
- [9] Alnes H, Amarzguioui M, Grøn Ø 2006 *Phys. Rev. D* **73** 08351
- [10] Alnes H, Amarzguioui M 2007 *Phys. Rev. D* **75** 023506
- [11] Bolejko K, Wyithe J S B 2009 *J. Cosmol. Astropart. Phys.* JCAP02(2009)020
- [12] Clifton T, Ferreira P G, Zuntz J 2009 *J. Cosmol. Astropart. Phys.* JCAP07(2009)029
- [13] Alexander S, Biswas T, Notari A, Vaid D 2009 *J. Cosmol. Astropart. Phys.* JCAP09(2009)025
- [14] Zibin J P, Moss A, Scott D 2008 *Phys. Rev. Lett.* **101** 251303
- [15] Clarkson C, Regis M 2010 The Cosmic Microwave Background in an Inhomogeneous Universe - why void models of dark energy are only weakly constrained by the CMB *Preprint* arXiv:1007.3443
- [16] Yoo C-M, Nakao K-i, Sasaki M 2010 *J. Cosmol. Astropart. Phys.* JCAP07(2010)012
- [17] Moss A, Zibin J P, Scott D 2010 Precision Cosmology Defeats Void Models for Acceleration *Preprint* arXiv:1007.3725
- [18] Biswas T, Notari A, Valkenburg W 2010 *J. Cosmol. Astropart. Phys.* JCAP11(2010)030
- [19] Wang Y, Mukherjee P 2007 *Phys. Rev. D* **76** 103533
- [20] Elgarøy Ø, Multamäki T 2007 *Astron. Astrophys.* **471** 65
- [21] Sachs R K 1961 *Proc. Roy. Soc. London A* **264** 309
- [22] Kristian J, Sachs R K 1966 *Astrophys. J.* **143** 379
- [23] Kantowski R, Vaughan T, Branch D 1995 *Astrophys. J.* **447** 35
- [24] Marra V, Kolb E W, Matarrese S, Riotto A 2007 *Phys. Rev. D* **76** 123004

- [25] Marra V, Kolb E W, Matarrese S 2008 *Phys. Rev. D* **77** 023003
- [26] Kainulainen K, Marra V 2009 *Phys. Rev. D* **80** 127301
- [27] Brouzakis N, Tetradis N, Tzavara E 2007 *J. Cosmol. Astropart. Phys.* JCAP02(2007)013
- [28] Brouzakis N, Tetradis N, Tzavara E 2008 *J. Cosmol. Astropart. Phys.* JCAP04(2008)008
- [29] Vanderveld R A, Flanagan É É, Wasserman I 2008 *Phys. Rev. D* **78** 083511
- [30] Valkenburg W 2009 *J. Cosmol. Astropart. Phys.* JCAP06(2009)010
- [31] Szybka S J 2010 arXiv:1012.5239
- [32] Clifton T, Zuntz J 2009 *Mon. Not. R. Astron. Soc.* **400** 2185
- [33] Clifton T, Ferreira P G 2009 *Phys. Rev. D* **80** 103503
- [34] Bolejko K 2011 *Astron. Astroph.* **525** A49
- [35] Bolejko K 2010 *Mon. Not. R. Astron. Soc.* in press, Preprint arXiv:1011.3876
- [36] Lewis A, Challinor A 2006 *Phys. Rep.* **429** 1
- [37] Hanson D, Challinor A, Lewis A 2010 *Gen. Rel. Grav.* **42** 2197
- [38] Ellis G F R 1971 in *Proceedings of the International School of Physics ‘Enrico Fermi’, Course 47: General Relativity and Cosmology*, ed. R. K. Sachs. Academic Press, New York and London, pp. 104 – 182; reprinted, with historical comments, in 2009 *Gen. Rel. Grav.* **41** 581
- [39] Dyer C C, Roeder R C, 1972, *Astrophys. J.* **174** L115
- [40] Dyer C C, Roeder R C 1973 *Astrophys. J.* **180** L31
- [41] Mattsson T 2010 *Gen. Rel. Grav.* **42** 567
- [42] Pyne T, Birkinshaw M 2004 *Mon. Not. R. Astron. Soc.* **348** 581
- [43] Bonvin C, Durrer R, Gasparini M A 2006 *Phys. Rev. D* **73** 023523
- [44] Hui L, Greene P B 2006 *Phys. Rev. D* **73** 123526
- [45] Enqvist K, Mattsson M, Rigopoulos G, 2009 *J. Cosmol. Astropart. Phys.* JCAP09(2009)022
- [46] Kainulainen K, Marra V 2009 *Phys. Rev. D* **80** 123020
- [47] Kainulainen K, Marra V 2011 arXiv:1011.0732
- [48] Yu H-R, Lan T, Wan H-Y, Zhang T-J, Wang B-Q 2010 *Research Astron. Astrophys.* in press; arXiv:1008.1935
- [49] Lemaître G 1933 *Ann. Soc. Sci. Bruxelles A* **53** 51 (English translation, with historical comments: 1997 *Gen. Rel. Grav.* **29** 637)
- [50] Tolman R C 1934 *Proc. Nat. Acad. Sci. USA* **20** 169 (reprinted, with historical comments: 1997 *Gen. Rel. Grav.* **29** 931)
- [51] Lewis A, Challinor A, Lasenby A 2000 *Astrophys. J.* **538** 473
- [52] Amanullah R, Lidman C, Rubin D, Aldering G, Astier P, et al 2010 *Astrophys. J.* **716** 712
- [53] Weinberg S 1976 *Astrophys. J.* **208** L1
- [54] Ellis G F R, Bassett B A C C, Dunsby P K S 1998 *Class. Quantum Grav.* **15** 2345
- [55] Peebles P J E 2010 *AIP Conference Proceedings* **1241** 175
- [56] Kayo I, Taruya A, Suto Y 2001 *Astrophys. J.* **561** 22
- [57] Lahav O, Suto Y 2004 *Living Rev. Relat.* **7** 8 [Online article]: cited on 27/09/2010, <http://www.livingreviews.org/lrr-2004-8>
- [58] Peebles, P. J. E. (1980). *The Large-Scale Structure of the Universe*. Princeton: Princeton University Press
- [59] Krasiński A 1997 *Inhomogeneous Cosmological Models* (Cambridge: Cambridge University Press)
- [60] Plebański J, Krasiński A 2006 *An Introduction to General Relativity and Cosmology* (Cambridge: Cambridge University Press)
- [61] Bolejko K, Krasiński A, Hellaby C, Célérier M N 2009 *Structures in the Universe by exact methods: formation, evolution, interactions* (Cambridge: Cambridge University Press)

## Appendix A. Construction of model Len 1

In order to solve (6) one needs to know  $\nabla^2\phi$  along the line of sight. Using the Poisson equation the gravitational potential is related to density fluctuations. Therefore, a method of generating density fluctuations is needed. In the non-linear regime, the density fluctuations are not Gaussian (there is no symmetry as  $-1 \leq \delta < \infty$ ). However, in the non-linear regime the distribution of density fluctuations can be approximated with the one-point log-normal PDF [56, 57]

$$P(\delta) = \frac{1}{\sqrt{2\pi\sigma_{nl}^2}} \exp\left[-\frac{(\ln(1+\delta) + \sigma_{nl}^2/2)^2}{2\sigma_{nl}^2}\right] \frac{1}{1+\delta}, \quad (\text{A.1})$$

where

$$\sigma_{nl}^2 = \ln[1 + \sigma_R^2], \quad \text{and} \quad \sigma_R^2 = \frac{1}{2\pi^2} \int_0^\infty dk \mathcal{P}(k) W^2(kR) k^2, \quad (\text{A.2})$$

and  $\mathcal{P}(k)$  is the matter power spectrum. Therefore, the algorithm for  $\delta$  along the line of sight is as follows:

- (i) The radius of a structure  $R$  is randomly generated from a uniform distribution, from 0 to 10 Mpc.
- (ii) Then  $\sigma_R$  is calculated using (A.2).
- (iii) An initial value of a density fluctuation  $\delta_0$  is generated from the log-normal distribution (A.1).
- (iv) The evolution of  $\delta$  (at a fixed point) is calculated using the linear approximations [58]

$$\ddot{\delta} + 2\frac{\dot{a}}{a}\dot{\delta} = \frac{4\pi G}{c^2}\rho\delta. \quad (\text{A.3})$$

- (v) Using the Poisson equation,  $\nabla^2\phi$  is calculated and inserted into (7) which is solved from  $\chi_i$  to  $\chi = \chi_i + \chi(2R)$ .
- (vi) Steps (i)–(v) are repeated so (7) is solved from  $\chi = 0$  to  $\chi_e$ .

A sample of density fluctuations along the line of sight is presented in Figure 1.

## Appendix B. Construction of model Len 2

Instead of using directly the log-normal distribution to generate density fluctuations along the line of sight an alternative approach is used. In [35] it was shown that compensated structure can also have a log-normal PDF. Thus, Len 2 generates density fluctuations along the line of sight using a method discussed in [35]. The algorithm is as follows:

- (i) First the radius of a void  $R_v$  is generated from the Gaussian distribution with the mean of 12 Mpc and the standard deviation of 2 Mpc.

- (ii) Density within the void  $\Omega_v$  is generated from the Gaussian distribution with the mean  $0.2\Omega_m$  and  $\sigma = 0.27\Omega_m$ . If a generated in this way  $\Omega_v$  is lower than  $0.01\Omega_m$  then the generation is repeated. If after 6 times it is still less than  $0.01\Omega_m$  then  $\Omega_v$  is generated for a uniform distribution between 0 and  $0.01\Omega_m$ . If  $\Omega_v \geq \Omega_m$  then  $\Omega_v$  is generated one more time. If after 6 times  $\Omega_v \geq \Omega_m$  then its value is chosen for a uniform distribution from  $0.85\Omega_m$  to  $\Omega_m$ . Density contrast is then  $\delta = \Omega_v/\Omega_m - 1$ .
- (iii) Density of the surrounding shell  $\Omega_s$  is generated from the Gaussian distribution with the mean of  $1.75\Omega_m$  and  $\sigma = 0.7\Omega_m$ . If  $\Omega_s \leq \Omega_m$  then its value is generated again. If after 6 times  $\Omega_s \leq \Omega_m$  then its value is generated for a uniform distribution between  $1.75\Omega_m$  and  $1.95\Omega_m$ . Density contrast is then  $\delta = \Omega_s/\Omega_m - 1$ .
- (iv) The condition, that the structure is compensated implies that the radius of the whole structure is

$$R = R_v \left( \frac{\Omega_s - \Omega_v}{\Omega_s - \Omega_m} \right)^{1/3} .$$

- (v) The angle at which the light ray enters the structure is generated from a uniform distribution between 0 and  $0.25\pi$ .
- (vi) The evolution of  $\delta$  (at a fixed point) was calculated using (A.3).
- (vii) Integral (7) is solved from  $\chi_i$  to  $\chi_f$  (where  $\chi_i$  is the comoving coordinate of the entry point and  $\chi_f$  the point where the light ray exits the structure).
- (viii) Steps (i)–(vii) are repeated so (7) is solved from  $\chi = 0$  to  $\chi_e$ .

A sample of density fluctuations along the line of sight is presented in Figure 1. The reason for defining the profile as above is to have a profile that allows for some kind of randomness (the size and the density of voids and shells is random), but still because we use spheres (which suppose to correspond to real wall that surround real voids) the fluctuations are not purely random – the pure randomness is gone once we decided to use spheres. Still because of the above construction the 3D density PDF of this model is almost log-normal. (see [35] for a discussion). If instead of the Gaussian, the uniform PDF is used (steps (i)–(iii)) then the PDF of  $\delta$  is not log-normal PDF.

### Appendix C. Construction of model Len 3

- (i) First the radius of a void  $R_v$  is generated from a uniform distribution between 0 and 30 Mpc.
- (ii) Density contrast of the void  $\delta_v$  is generated from a uniform distribution between  $-0.5$  and  $-1$ .
- (iii) Integral (7) is solved from  $\chi_i$  to  $\chi_f$  (where  $\chi_i$  is the comoving coordinate of the entry point and  $\chi_f$  the point where the light ray exits the void).
- (iv) Then the length of a filament  $L_f$  is generated from a uniform distribution between 0 and 5 Mpc.

- (v) The density contrast of the filament  $\delta_f$  is generated from a uniform distribution between 0.5 and 2.5.
- (vi) Integral (7) is solved from  $\chi_i$  to  $\chi_f = \chi_i + \chi(L_f)$ .
- (vii) Steps (i)–(vi) are repeated so (7) is solved from  $\chi = 0$  to  $\chi_e$ .

A sample of density fluctuations along the line of sight is presented in Figure 1.

## Appendix D. Construction of the Swiss Cheese model

The Swiss Cheese model considered here is based on the Lemaître-Tolman (LT) model [49, 50], which is the simplest generalization of the Friedmann models. The metric of the LT model is

$$ds^2 = dt^2 - \frac{R_{,r}^2}{1 + 2E} dr^2 - R^2(t, r) (d\vartheta^2 + \sin^2 \vartheta d\varphi^2), \quad (\text{D.1})$$

where  $E(r)$  is an arbitrary function. In the Friedmann limit  $E \rightarrow -k_0 r^2$  (in a general LT model the ‘curvature index’ is position dependent).  $R(t, r)$  is the areal distance and in the Friedmann limit  $R \rightarrow ra(t)$  (in a general LT model the scale factor is position dependent). The evolution (i.e. the generalized Friedmann equation) is

$$\dot{R}^2 = 2E + \frac{2M}{R} + \frac{\Lambda}{3} R^2, \quad (\text{D.2})$$

$M(r)$  is an arbitrary function defined by the mass density:

$$\kappa\rho = \frac{2M_{,r}}{R^2 R_{,r}}. \quad (\text{D.3})$$

From (D.2) the age of the Universe,  $\tau$ , is

$$\tau(r) = t - t_B(r) = \int_0^R \frac{d\tilde{R}}{\sqrt{2E + 2M/\tilde{R} + \frac{1}{3}\Lambda\tilde{R}^2}}, \quad (\text{D.4})$$

where  $t_B(r)$  is an arbitrary function and in the Friedmann model  $t_B \rightarrow \text{const}$  (in a general LT model the age of the universe is position dependent). There are three arbitrary functions in the LT model  $t_B(r)$ ,  $M(r)$ , and  $E(r)$ , however only 2 are physically independent. For a review of different applications of the LT models see [59, 60, 61]. Here we will assume that the model is defined by the assumption that the age of the universe is everywhere the same,  $t_B = 0$  and the function  $M(r)$  is

$$M = M_0 + \begin{cases} M_1 \ell^3 & \text{for } \ell \leq x_a, \\ M_2 \exp \left[ - \left( \frac{\ell - 2x_a}{x_a} \right)^2 \right] & \text{for } x_a \leq \ell \leq 3x_a \\ -M_1 (\ell - 4x_a)^3 & \text{for } 3x_a \leq \ell \leq 4x_a, \\ 0 & \text{for } \ell \geq 4x_a, \end{cases} \quad (\text{D.5})$$

where  $\ell = r/\text{kpc}$ ,  $M_0 = (4\pi G/3c^2)\rho_b \ell^3$ ,  $\rho_b = \Omega_m \frac{3H_0^2}{8\pi G}$ ,  $\Omega_m = 0.262$ ,  $H_0 = 71.4 \text{ km s}^{-1} \text{ Mpc}^{-1}$ ,  $M_1 = x_a^{-3} M_2 e^{-1.5}$ ,  $M_2 = 3.29 \times 10^{10} \text{ kpc}$  and  $-2.91 \times 10^{11}$  for regions A and B

respectively,  $x_a = 5 \times 10^3$  and  $15 \times 10^3$ , for regions A and B respectively. Region A and B are matches alternately at  $r = 4x_a$ . The above profile was chosen for the following reasons: it behaves like a FLRW model for  $\ell \leq x_a$  but with lower density than outside, then for  $x_a \leq \ell \leq 3x_a$  we have a transition region, and a cubic behavior for  $3x_a \leq \ell \leq 4x_a$  allows for a smooth matching to the background values. Density fluctuations along the line of sight are presented in Figure 1. It should now be clear why we have selected the above set of functions. These functions allow us to obtain the present-day density profile as presented in Figure 1. This model has thus 2 advantages: 1) it allows to calculate the evolution and the distance exactly, without additional approximations, 2) the mean of the density fluctuations along the line of sight is zero, i.e. as in Len 1 model and unlike in Len 2 and Len 3 models.

When constructing a Swiss Cheese model, the junction conditions need to be satisfied. Here we match the LT inhomogeneity (holes) to the Friedmann background (cheese). The LT patches are placed so that their boundaries touch wherever a light ray exits one inhomogeneous patch. Thus, the ray immediately enters another LT patch and does not spend any time in the Friedmann background. To match the LT patch to the Friedmann background across a comoving spherical surface,  $r = \text{constant}$ , the conditions are: 1) the mass inside the junction surface in the LT patch is equal to the mass that would be inside that surface in the homogeneous background; 2) the spatial curvature at the junction surface is the same in both the LT and Friedmann models, which implies that  $E(r) = -k_0 r^2$  and  $E' = -2k_0 r$ ; 3) the bang time and  $\Lambda$  must be continuous across the junction. As seen, by the construction these conditions are satisfied.

Finally, the redshift is given by [61]

$$\begin{aligned} \frac{dr}{dz} &= \pm \frac{1}{1+z} \frac{\sqrt{1+2E}}{\dot{R}}, \\ \frac{dt}{dz} &= \frac{1}{1+z} \frac{R'}{\dot{R}}. \end{aligned} \tag{D.6}$$

Only radial geodesic (i.e. the geodesics that propagate through the origin) will be considered. In such a case the shear of light bundle is zero [27, 28]. Thus, the junction of null geodesics only requires the matching of one of the components of  $k^\alpha$  as the other one is given from  $k^\alpha k_\alpha = 0$ .